Length Scale Dependent Probe Diffusion in Drying Acrylate Latex Films

ARTICLE *in* MACROMOLECULES · JANUARY 2002

Impact Factor: 5.8 · DOI: 10.1021/ma010531n

Length Scale Dependent Probe Diffusion in Drying Acrylate Latex Films

A. Veniaminov,‡ T. Jahr,† H. Sillescu,† and E. Bartsch*,†

Institut für Physikalische Chemie, Johannes Gutenberg-Universität, Jakob-Welder-Weg 15, D-55099 Mainz, Germany; and S. I. Vavilov Optical Institute, Birzhevaya line 12, St. Petersburg 199034, Russia

Received March 28, 2001; Revised Manuscript Received October 30, 2001

ABSTRACT: Applying forced Rayleigh scattering to monitor the drying behavior of poly(*n*-butyl-methacrylate-*co*-acrylic acid) dispersions ($T > T_g + 5$ K) via the diffusion of a hydrophobic dye, we find a characteristic length scale dependence of the tracer diffusion coefficient $D_{app}(\Lambda)$ ($\Lambda = 0.17-10$ μm), which allows one to quantitatively describe the transition from a wet, inhomogeneous to a dry, homogeneous polymer latex film within a two-state diffusion model. $D_{app}(\Lambda)$ showed an enhancement of up to 2 orders of magnitude when increasing the length scale. These findings can be quantitatively rationalized within the two-state model assuming Fickian diffusion proceeding slowly in the latex cores and fast diffusion in a heavily plasticized, interfacial phase. From the water content dependence of the model parameters we conclude that the drying process proceeds first by exclusive water loss from the interfacial phase, while the properties of the particle cores remain unchanged. When the Λ dependence of $D_{app}(\Lambda)$ disappears, water withdraws also from the cores and a homogeneous polymer film forms. Our approach allows one to quantitatively follow property changes in the different compartments of a drying latex dispersion.

1. Introduction

The formation of homogeneous void-free polymer films from concentrated dispersions of polymer colloids (also called latex) has become the major process to produce coatings nowadays used in paints, dirt and water repellent textiles, as adhesives and in papermaking. A strong incentive for the replacement of solvent-based coatings with waterborne ones has been to cut down on the use of volatile organic components (VOC) for environmental and economical reasons. Even waterborne coatings still contain significant amounts of VOC as coalescing aids. Thus, the continued pressure to further reduce emissions and the concomitant need for improved coatings has led to a renaissance of interest in the mechanism of film formation.[1−5]

Film formation is a complex process occurring in a highly heterogeneous sample, which consists of compartments (polymer phase, water phase, and the interface region which sometimes is addressed as hydrophilic membrane in the literature[6]) with differing microscopic properties giving rise to heterogeneous distributions of features such as, e.g., microviscosity, surfactant, and additive concentrations. Many of the early studies on film formation were based on techniques that probed properties averaged over the whole film, providing large-scale macroscopic information only. In addition, as the majority of the early work was done with industrial applications in mind, widely varying film forming conditions and latex formulations were employed. Thus, it is not surprising that a unified picture of the film formation mechanism and its driving forces was missing and many controversies existed.[5]

Only in the past decade significant progress toward what may be called a standard model of film formation has been achieved.[3,5,6] This has been mainly due to the focus of experimental work on a few standard latex systems, poly(*n*-butyl methacrylate) (PBMA) being the most prominent one,[2] and controlled film forming conditions as well as to a shift to noninvasive techniques such as small angle neutron scattering,[6−12] nonradiative energy transfer[13−15] and atomic force microscopy[16−20] which provided insight into structural details and dynamical processes on microscopic length scales. According to this standard model, film formation proceeds in three stages: in stage I water loss on drying a latex dispersion leads to a close packing of spheres. On further water loss (stage II) the particles deform (in case the temperature is above the so-called MFT = minimal film-forming temperature), eventually leading to a space-filling arrangement of rhombododecaeders of polymer material separated by more or less hydrophilic interfaces. The latter form a percolated network containing the hydrophilic components (rest water, surfactant, ionic additives, surface charges, etc.), which may act as a channel system allowing for transport of water. During this stage the film becomes transparent when the size of interstitial water areas becomes significantly smaller than the wavelength of visible light. Stage III is characterized by interdiffusion of polymer chains between neighboring particles (if the temperature is above the polymer glass transition temperature T_g) with a concomitant loss of particle individuality, thereby imparting mechanical strength to the formed film.

While recent developments have emphasized structural information and polymer dynamics there is a need for further experiments probing especially the transport properties of nascent films, preferably with spatial resolution. One step in this direction is the application of tracer techniques that are able to selectively monitor the transport or dynamic properties of one specific compartment of a nascent film by a judicious choice of probe molecules and to provide complementary information, e.g., on water loss and surfactant mobility or

* To whom all correspondence should be addressed. E-mail: bartsch@aak.chemie.uni-mainz.de.
† Johannes Gutenberg-Universität.
‡ S. I. Vavilov Optical Institute.

10.1021/ma010531n CCC: $22.00
Published on Web 01/03/2002

polymer diffusion, as has been suggested recently.[21] The conceptually simplest experiment is to add a probe molecule to a dispersion and to address it to a specific compartment by tuning its hydrophilicity through chemical modification. To study the changes of the target compartment during film formation one then needs a method sensitive enough to monitor the motion of the probe molecule. A technique fulfilling these requirements is forced Rayleigh scattering (FRS),[22] a holographic method which allows one to measure the tracer diffusion coefficient of a photoreactive dye molecule or of species that are labeled by it through chemical attachment. The technique is particularly suited to monitor slow diffusion processes[23] covering diffusion coefficients in the range 10^{-13}–10^{-21} m^2 s^{-1} and has been successfully used in the past to study polymer diffusion in melts,[24] colloid diffusion in highly concentrated dispersions,[25] and the role of small molecule additives in polymers[26–28] as well as diffusion close to and below the glass transition temperature.[29–33] In recent studies of block copolymer melts its applicability to diffusion in heterogeneous systems has been shown.[34–39]

In this report, we want to demonstrate that FRS can be profitably applied to nascent films formed on drying aqueous dispersions of polymer colloids, allowing one to quantitatively follow the drying process and the concomitant changes of transport properties of the polymer phase and the hydrophilic interface by a two-state diffusion model.

2. Experimental Section

2.1. Forced Rayleigh Scattering Measurements. The basic idea of the forced Rayleigh scattering (FRS) technique[22] consists of imprinting a photoinduced periodical structure—a holographic grating—into the volume of the sample, followed by monitoring the light diffracted from such a grating. The efficiency of diffraction is determined by spatial modulation of optical parameters (refractive index, absorption coefficient). In this work, we deal with holographic gratings recorded in the bulk of polymer samples by permanent photochemical change induced by photobleaching a suitable dye molecule (see section 2.2). Thus, the spatial modulation of the optical parameters directly depends on the spatial modulation of the concentrations of photobleached and unbleached dye. Diffusion of the dye molecules leads to the disappearance of the holographic grating, which is monitored in FRS experiments as a diffraction efficiency relaxation curve. From the relaxation time, τ, the tracer diffusion coefficient can be derived. Since in this technique the spatial scale of diffusional measurements, given by a grating distance Λ, can be smaller than the light wavelength, determination of very small diffusion coefficients down to 10^{-21} m^2 s^{-1} becomes feasible. Λ can be—loosely speaking—looked upon as a kind of yardstick over which tracer diffusion is monitored. Thus, any Λ-dependence of the transport properties seen in FRS experiments can provide valuable information about the length scale of spatial inhomogeneities in nascent films as will be shown later. More details about basic principles and applications of FRS are described in the literature.[22–25,29,30]

The instrumentation used for this study was basically the same as in refs 23 and 24. An Argon ion laser (Coherent Innova-90; wavelength λ = 488 nm, run at 100–200 mW output power) or, alternatively, a continuous wave Nd:YAG laser (Coherent-532–30; λ = 532 nm, ~20 mW) was used as the source for writing as well as reconstructing the holographic grating. The results were checked to be uninfluenced by the laser choice. The spot size of the photoinduced gratings was 0.5 to 1 mm in diameter. By changing the angle 2Θ between the writing beams the grating distance, Λ, was varied from 0.34 to 20 μm in transmission geometry ($\Lambda = \lambda/2(\sin\Theta)$) and from 0.16 to 0.2 μm in reflection geometry of the optical scheme ($\Lambda = \lambda/2(n^2 - \cos^2\Theta)^{1/2}$, where n denotes the refractive index of the probed material).

The samples were placed in the FRS cuvette, which consists of a brass frame with two parallel quartz windows.[24] To ensure water-tightness of the cuvettes two Teflon rings or rubber O-rings were inserted between the quartz windows and the brass body. No spacer was placed between the windows; the sample itself served as such, due to its own rigidity. To confirm the absence of water loss during a series of measurements, which could last from hours to days, reproducibility of FRS kinetics was checked several times in the course of an experiment. In addition, the weight of the sample was controlled before and after optical measurements to keep track of the water content of the films. To estimate the integral rest water content, the samples were also weighed after complete drying under vacuum. Since, due to surface tension, the films dried not uniformly, these estimates differ from the local water concentrations in the spots where the photoinduced gratings were created. Positioning the grating at different spots of the sample showed variations of the decay time τ. In the worst case, corresponding to intermediate water concentrations, the relaxation times varied by about a factor of 2, the smaller τ values being obtained for the thinner central area. In the case of very wet (~20% weight per weight water) or dry films, this macroscopic inhomogeneity of the samples disappeared and the variation of relaxation times was found to be within the error margin of ±10%, typical for standard FRS experiments on homogeneous samples. To avoid problems due to this macroscopic heterogeneity, systematic measurements were performed within a ring area at a distance of 5–8 mm from the center of the sample; with this precaution the reproducibility of the results was satisfactory. To avoid nonequilibrium effects due to macroscopic flow induced by water redistribution after stopping the drying process, the samples were equilibrated in the setup at the drying temperature of 40 °C (= T_g + 5 °C). The FRS measurements were performed at 40 °C as well, to avoid complications of the FRS kinetics due to aging effects that typically appear close above and below T_g.

2.2. Tracer Dye. The application of the FRS technique to selectively study the transport properties of specific compartments of a multicompartment system like a film-forming latex dispersion imposes some special requirements on the choice of the photoreactive dye: (i) As in the initial stages of the film formation the nascent film is generally rather turbid, a high signal-to-noise ratio is necessary. To avoid plasticization of the polymer material by the dye molecules[26,28] concentrations should be well below 1 % w/w (weight per weight) of dye. (ii) It should be possible to selectively address the dye to a specific compartment, e.g., via its hydrophilicity. For the initial FRS studies of colloidal film formation the photochromic fulgide dye Aberchrome540 (α-2,5-dimethyl-3-furylethylidene(isopropylidene)succinic anhydride, **1**), was chosen as a hydrophobic

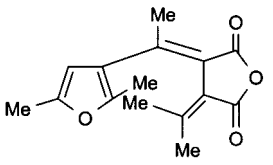

1

tracer. Thus, the tracer was expected to predominantly probe the polymer phase of a nascent film. Its photochemistry is described elsewhere[40–43] as well as its use as a FRS tracer.[30,44] Among the advantages of Aberchrome-540 (ACR) are strong photoinduced changes of the optical properties, ensuring high diffraction efficiencies (>10% measured at 633 nm) achievable at moderate tracer concentrations (<0.5% w/w), as well as good photoreversibility and thermostability. For a few comparative experiments the samples were also prepared with the photochromic dyes tetrahydrothiophene–indigo derivative (TTI)[30] and 9,10-phenanthrenequinone (PQ).[44]

2.3. Latex Preparation. Latex particles were prepared by semicontinuous emulsion polymerization using sodium per-

Table 1. Composition and Characterization of Studied Latex Dispersions[a]

monomer composition	P(BMA) 100% BMA	P(BMA-*co*-1%AA) 99% BMA, 1%AA			P(BMA-*co*-5%AA) 95% BMA, 5%AA	P(BMA-*co*-10%AA) 90% BMA, 10%AA
R(CHDF)/nm	107	101	169	41	105	102
σ(CHDF)/%	6.7	4.4	8.4	13.8	6.5	7.3
solid content/%	28.0	28.9	30.2	29.5	29.7	28.9
T_g/°C	35	35	36	38	38	
MFT/°C	27	32	28	26	32	32

[a] Monomer composition gives the weight ratio of *n*-butyl methacrylate (BMA) and acrylic acid (AA) as used in the semicontinuous emulsion polymerization. R(CHDF) and $\sigma = \sqrt{(\langle R^2\rangle - \langle R\rangle^2)}/(R\times 100)$are the particle radii and the size polydispersities as determined by capillary hydrodynamic fractionation. Solid content was determined gravimetrically after drying to weight constancy at 100 °C. Glass transition temperature T_g of the resulting polymer films was determined with differential scanning calorimetry, whereas the minimum film-forming temperature (MFT) was determined on a MFT bank.

sulfate (Riedel de Haïn) as initiator. The monomers *n*-butyl methacrylate (BMA) and acrylic acid (AA) were of p.a. grade. Sodium dodecyl sulfate (SDS, Henkel) was used as an emulsifying agent with a molar ratio of 1:200[67] with respect to monomer concentration. All emulsion polymerizations were carried out in deionized water. The resulting dispersions were deodorized with hydrogen peroxide (Merck) and ascorbic acid (Merck) yielding a pH of 7.5 after neutralization with sodium hydroxide (Baker). The residual monomer content was below 300 ppm. Where necessary, remaining traces of peroxides (about 10 mg H_2O_2/L as determined by Merckoquant test strips) were removed by adding an appropriate amount of sodium sulfite. By varying the initial mixture of SDS, water, and sodium persulfate it was possible to gain control over the number of initiating particles thus allowing one to change the particle diameters as discussed below.

Particle radii R and polydispersities $\sigma = (\langle R^2\rangle - \langle R\rangle^2)^{1/2}/\langle R\rangle$ were determined by capillary hydrodynamic fractionation (CHDF-1100 (Fa. Matec)).[46] The glass transition temperature of the dry polymer, T_g, was measured by differential scanning calorimetry (Mettler Toledo Star System) at a scanning rate of 10 K/min in a range from −50 to +100 °C. The minimum film formation temperature (MFT) was determined employing a Thermostair film formation bank (from Coesfeld, Dortmund, Germany). The wet film thickness was 100 μm, and the MFT was read off after a drying time of 24 h. To check the proposed diffusion model (see below) for analyzing the FRS experiments three sizes of latex particles consisting of BMA copolymerized with 1% w/w of acrylic acid P(BMA-*co*-1%AA) were studied.

In addition, a dispersion of pure P(BMA) and dispersions with higher acrylic acid content (5% and 10% w/w) were employed to demonstrate the ability of our approach to yield information on the effect of changing the formulation of the dispersion (the hydrophilicity of the polymer). The most relevant information concerning the dispersions studied is given in Table 1. Unless stated otherwise, the samples made of poly(BMA-*co*-1%AA) with particle size 100 nm were used in the experiments.

2.4. Film Preparation. The photochromic dye was added in crystalline form to the aqueous dispersion (yielding tracer concentrations below 0.5% w/w in the completely dried polymer film), which was then stirred. After 12 h, the hydrophobic dye tracer was completely absorbed by the particles.

To prepare films suitable for FRS experiments a few drops of the emulsion were pipetted onto the warm quartz window (Hellma Quartz-Suprasil 1; 2 cm in diameter) of a FRS cuvette and dried at a temperature of 40 °C. If the upper surface of the emulsion was left open, the drying process developed from the outer circle to the center and from top to bottom. Due to the increase of concentration of the solid phase in the outer ring, the central area of the film became thinner, hence drying faster, and at a certain intermediate stage appeared drier than the peripheral area. When the sample appeared slightly transparent, but stayed relatively soft (∼20% w/w water), another quartz window was placed on top of the film and the whole sandwich screwed in the cuvette frame in order to form a flat upper polymer surface and prevent further drying. Applying only moderate pressure, it was often only possible to flatten the outer ring area (∼5 mm width) of the sample, whereas the central area was thinner and had a rough surface. After the preparation itself, the samples were kept in the cuvette at 40 °C during a few hours for equilibration and for obtaining a smooth interface between the polymer surface and the top quartz window.

To achieve lower concentrations of water, the cuvette was afterward disassembled, the upper window removed from the already formed surface and the drying process continued. This was feasible as at a drying temperature of 40 °C, being 5 °C above T_g of the dry polymer, the polymer in the wet films was sufficiently well plasticized with residual water.

To determine the rest water contents of the samples, each sample was dried to weight constancy under vacuum (typically a day) after the measurements. The integral water content of wet films was then determined gravimetrically with an estimated error of ±0.5% w/w. The dry films obtained had a thickness of ∼0.2 mm. Refractive indexes of the films, as measured with an Abbe refractometer, changed with drying from 1.451 (18% water) to 1.477 (dry film).

To isolate the effect of the hydrophilic material in the emulsions and that of the specific architecture of latex films we also examined samples prepared from the pure polymer produced in these polymerizations. For this purpose, the dispersion was coagulated by freezing or water evaporation. The polymer was then purified by repeatedly dissolving it in THF and subsequent precipitation from water. After addition of the dye tracer, the polymer was finally freeze-dried from a benzene solution. Films were prepared by either melt-pressing the polymer powder or casting from a concentrated toluene solution.

2.5. Primary Evaluation of FRS Data. Being a holographic technique, FRS requires a certain optical quality of the material under investigation. This study only covers relatively late stages (less than 20% w/w of water), where the samples appeared reasonably transparent notwithstanding the considerable amount of residual water. The holographic grating, in principle, results from a periodic spatial modulation of the refractive index (phase grating) and the absorption constant (amplitude grating) of the dye tracer and its photo product, respectively. Thus, the refractive index modulation, $\Delta n(x,t)$ (or the absorption coefficient modulation $\Delta\kappa(x,t)$), is proportional to that of the excess concentration $\Delta C(x,t)$ of the unbleached dye, which decays by the diffusion component across the grating (along the x-axis).

At the first step of a FRS measurement, a holographic grating is produced in the sample by two interfering laser beams. Although the grating period is in certain cases even smaller than the particle size (180 nm for reflection grating vs 200 nm diameter), both the diameter and thickness of the gratings exceed the grating period and the particle size by several orders of magnitude (the gratings extend over at least 10^9 particles). Thus any local inhomogeneities of the dye distribution on the length scale of the particle size are averaged over and the gratings can be described by a sinusoidal spatial distribution of concentrations:

$$C(x,t=0) = C_0 - {}^1/_2\Delta C(x,t) = C_0 - {}^1/_2\Delta C(t=0)(1+\cos(q_\Lambda x)), \quad (1)$$

where

$$q_\Lambda = 2\pi/\Lambda = (4\pi/\lambda)\sin(\Theta) \quad (2)$$

is the grating vector, Λ denotes the grating distance (spatial period), C_0 is the initial (uniform) dye concentration, $\Delta C(t)$ is the maximum depth of photoinduced modulation of concentration, λ and Θ are the wavelength and half of the writing beams crossing angle (both within the medium), respectively.

Supposing that the postexposure evolution of concentration is driven by Fickian diffusion, the grating concentration profile stays sinusoidal, with Λ unchanged, but the modulation depth $\Delta C(t)$ decays exponentially:

$$C(x,t) = C_0 - {}^1/_2\Delta C(t)(1 + \cos(q_\Lambda x)) \quad (3a)$$

$$\Delta C(t) = \Delta C(t=0)\exp(-Dq_\Lambda{}^2 t) = \Delta C(t=0)\exp(-t/\tau) \quad (3b)$$

Under the common "weak grating" assumption[22] the diffraction efficiency of the grating is proportional to the square of the modulation amplitude. Hence, the FRS signal is described by a single-exponential decay as well:

$$I(t) = I(0)(\exp(-t/\tau))^2 = I(0)\exp(-2t/\tau) = I(0)\exp(-8\pi^2 Dt/\Lambda^2) \quad (4)$$

Such strictly exponential decays were always observed in completely dried films at $T_g + 5$ K, irrespective of the chosen way of film preparation (see last section). Thus, complications arising from complementary gratings as discussed in the literature[47−49] can be excluded with good confidence for our dye/polymer system.

Whereas spatial heterogeneity does not affect the spatial modulation of optical properties of the medium by the grating, it influences the time dependence of the grating decay. Thus, in a spatially inhomogeneous medium the FRS decay becomes nonexponential since the diffusivity varies during the tracer motion across regions of high and low mobility. This situation is encountered in polymer materials close to the glass transition[23] and described by a distribution of relaxation times or diffusion coefficients. This distribution is commonly taken into account by approximating the time decay by a stretched exponential (Kohlrausch−Williams−Watts, KWW) instead of applying eq 4. Thus, the FRS intensity becomes

$$I(t) = I(0)(\exp(-(t/\tau)^\beta))^2, \quad (5)$$

where the stretching parameter, $\beta \leq 1$, is a measure of sample inhomogeneity. In case of Fickian diffusion the diffusion coefficient is given by

$$D = q_\Lambda{}^{-2}\langle\tau\rangle^{-1}, \quad (6)$$

where the average decay time is given by $\langle\tau\rangle = \tau\beta^{-1}\Gamma(\beta^{-1})$ and Γ is the gamma function.

To improve the signal-to-noise ratio in case of not completely transparent samples, it was desirable to increase the diffraction efficiency by applying stronger gratings. However, increasing the exposure was found to lead to progressive deviations of FRS decay curves from those corresponding to lower exposures, indicating that the weak grating approximation eq 5 is no longer applicable. In terms of KWW fit, both τ and β grow with exposure, the latter parameter in certain cases yielding unphysical values above 1. Thus, in case of stronger gratings, we used the Kogelnik formulas for the diffraction efficiency,[50,51] although the latter apply to idealized uniform infinite gratings; the next level of precision would require to take into account writing and reconstruction of the gratings with Gaussian beams.[52,53] As it was not clear, whether in case of Aberchrome the induced optical grating is predominantly due to a photochemical change either of the refractive index (giving rise to essentially a phase grating) or of the absorption coefficient (yielding essentially an amplitude grating) or of both (superposition of both types of gratings) we checked the two limiting cases. It turned out that a satisfactory description of the decay curves can be provided by replacing the basic KWW fit-function for FRS decay with the Kogelnik results for phase gratings:[50,51]

$$I(t) = \frac{I(0)}{\sin^2 A}\sin^2(A\exp(-(t/\tau)^\beta)) \quad \text{(for transmission phase gratings)} \quad (7)$$

$$I(t) = \frac{I(0)}{\tanh^2 A}\tanh^2(A\exp(-(t/\tau)^\beta)) \quad \text{(for reflection phase gratings).} \quad (8)$$

Both expressions degenerate to the simple KWW in the limit of weak grating ($A \rightarrow 0$; A represents the strength of the grating). This is demonstrated in Figure 1, where two decay curves obtained for different exposure times (20 ms and 100 ms) of hologram writing under otherwise identical conditions are compared. The longer exposure (100 ms) results in slower decay, $\tau = 122$ s, and a larger stretching parameter, $\beta = 1.03$, compared with $\tau = 104$ s and $\beta = 0.87$ for the exposure time of 20 ms, if the data are evaluated using eq 5. Application of the modified formula for transmission phase grating, eq 7, yields $\tau = 105$ s, $\beta = 0.93$ for 100 ms and $\tau = 103$ s, $\beta = 0.87$ for 20 ms exposure time where the latter agrees with the "weak grating" approximation within experimental accuracy; this is actually the test for the grating "weakness".

For amplitude transmission gratings, one would replace the sine in eq 7 by a hyperbolic sine. In our case, this procedure does not apply: the fits for the stronger grating in the given example yield $\tau = 123$ s and $\beta = 1.03$, values that do not improve upon the results from the linear approximation, eq 5. A more general fit-function, taking both phase and amplitude contributions into account, yields only a relatively weak amplitude component, responsible for a few percent of diffraction efficiency, and gives no further improvement, whereas uncertainty grows. Thus, for convenience the gratings produced in this work are assumed to behave as phase gratings. This may seem contradictory to the fact that the measurements are being performed within the absorption band of ACR. However, calculations based on Kramers−Kronig dispersion relations show that phototransformation of a fulgide dye can result in significant refractive index changes already within the absorption band of the colored form.[54] Certainly, the apparent applicability of our modified fit function in itself is not a definite proof of the phase nature of the gratings, even though such a result is consistent with the known photochemistry of the dye.[40−43]

To avoid artifacts due to the complication arising from the creation of strong gratings it was necessary to vary the exposure times during the FRS experiments and to apply both KWW and the appropriate exact fit-function in the treatment of the primary FRS data.

3. Strategy of Data Analysis − Models of Tracer Diffusion

To interpret the decay signals measured in the FRS experiments we considered two different possibilities with respect to the distribution of the hydrophobic tracer dye molecules in the nascent latex films: (i) exclusively in the polymer phase and (ii) between polymer phase and interfacial area. These two cases require application of different diffusion models for data analysis—the model of restricted or barrier-impeded diffusion for case i or the two-state model of diffusion for case ii.

The barrier-impeded diffusion model assumes that the motion of the hydrophobic dye is exclusively restricted to the polymer phase and that the hydrophilic particle/water interface represents a barrier to long distance transport of the dye. Thus, in stage I of the film

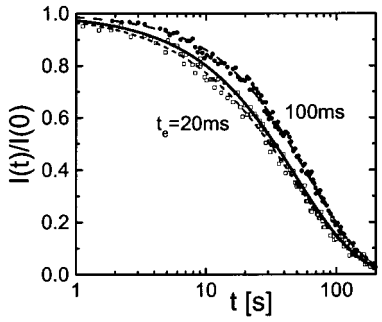

Figure 1. Normalized FRS intensity, $I/I(0)$, vs time, t, using the photoreactive dye Aberchrome-540 in molten P(BMA) at 40 °C and $\Lambda = 0.36\ \mu$m, with two different exposure times t_e, fitted the with stretched-exponential (KWW) function (eq 5) and modified functions for phase (eq 7) and amplitude gratings: (a) $t_e = 20$ ms (□), "weak grating", $\tau = 103$ (104) s, $\beta = 0.87$, regardless of the fit-function chosen; (b) $t_e = 100$ ms (●), "strong grating", $\tau = 122$ s, $\beta = 1.03$, giving a simple KWW fit; $\tau = 105$ s, $\beta = 0.93$, assuming phase grating (eq 7); $\tau = 126$ s, $\beta = 1.03$, using a similar formula for amplitude grating. The full line, approaching the kinetics of the weak grating, represents a simulation of KWW decay with the parameters τ, β obtained from fitting the data for strong grating with eq 7.

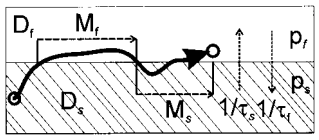

Figure 2. Schematic representation of the two-state model: The tracer molecule (○) experiences Fickian diffusion in two different phases (slow and fast phase, denoted s and f respectively) with the diffusion coefficients D_s and D_f. Mean exchange rates between the two phases are given by $1/\tau_s$ and $1/\tau_f$ corresponding to the mean residence times τ_s and τ_f in both phases before exchange. Root-mean-square displacements in the phases during residence times are $M_{s,f} = \sqrt{6D_{s,f}\tau_{s,f}}$. The relative probability densities of the tracer molecules in slow and fast compartments are given by p_s and p_f ($p_s + p_f = 1$) correspondingly.

formation (dense packing of the particles), the dye motion is restricted to diffusion in a sphere. Only in stage II, when particle coalescence starts and the polymer phases of neighboring particles become connected due to the disappearance of the interfaces, can the dye molecules perform diffusion over larger distances. In stage III, where the interfaces have completely vanished, dye motion should proceed by normal Fickian diffusion in a homogeneous polymer matrix. Thus, one would expect that in stage II the tracer diffusion coefficient is significantly reduced when the diffusional displacement exceeds particle size. However, as our experimental findings were clearly contrary to this prediction (see below), we will only discuss the two-state diffusion model in more detail.[68]

Two-State Model of Diffusion. The more general case, where the hydrophobic tracer moves through both the polymer phase and the interfacial region can be treated in the framework of a two-state model, which has been applied in the literature to pulsed field gradient NMR data monitoring diffusion of a probe in heterophase systems.[56,57] For this purpose, we assume an exchange process of the tracer molecules between the polymer phase, which we denote the "slow" state corresponding to slow diffusion, and the interfacial region, which is addressed as the "fast" state for reasons that will become clear below. A representative tracer molecule diffuse with a diffusion coefficient, D_s, for an average residence time, τ_s, inside the latex particle, and, subsequently, with a diffusion coefficient, D_f , for the average time, τ_f, in the interfacial region until it enters the interior of another latex particle etc.

Since we only measure diffusion along the x-direction across the holographic grating and neglect influences of tortuosity, the motion of a probe in film forming colloidal dispersions can be treated as a linear diffusion problem in terms of a simple two-state model, as shown schematically in Figure 2. Following Kärger et al.[56,57] the rate equations for Fickian diffusion and exchange are

$$(\partial/\partial t)P_s(x,t) = D_s(\partial^2/\partial x^2)P_s(x,t) - \tau_s^{-1}P_s(x,t) + \tau_f^{-1}P_f(x,t) \quad (9)$$

$$(\partial/\partial t)P_f(x,t) = D_f(\partial^2/\partial x^2)P_f(x,t) - \tau_f^{-1}P_f(x,t) + \tau_s^{-1}P_s(x,t), \quad (10)$$

where $P_i(x,t)$, i = s,f, denotes the probability density that the tracer has moved a distance x from its starting point in time t. Detailed balance requires that the mean residence times are related with the residence probabilities of tracer molecules in the "fast" and "slow" regions, p_f and p_s, by

$$\tau_s/\tau_f = p_s/p_f \quad (11)$$

and since $p_f + p_s = 1$ we obtain

$$p_f = \tau_f/(\tau_f + \tau_s); \quad p_s = 1 - p_f. \quad (12)$$

It should be noted that these residence probabilities are related to, but not identical with the volume fractions of the respective phases as the tracer dye may have different affinities (due to specific interactions) for them which would lead to differing p_s and p_f values even if the volume fractions were the same.

For further reference, we also introduce the mean squared displacements $\langle M^2\rangle$ that a tracer experiences within one phase before entering the other one:

$$\langle M_s^2\rangle = 6D_s\tau_s; \quad \langle M_f^2\rangle = 6D_f\tau_f. \quad (13)$$

The root-mean-square displacements $M_i = \langle M_i\rangle^{1/2}$, i = s, f, can be considered as a measure of the distance traveled by the tracer in a given phase within a residence time. With the initial conditions (i = s, f)

$$P_i(x,0) = a_i + b_i\cos(q_\Lambda x); \quad a_s/a_f = b_s/b_f = p_s/p_f \quad (14)$$

the observed FRS intensity is simply obtained from the Fourier transform of $P_s(x,t)$ and $P_f(x,t)$ at $q = q_\Lambda$, i.e., at the Bragg angle:

$$I(t) = I(0)P(q_\Lambda,t)^2 \quad (15)$$

Equations 9 and 10 are solved by Fourier transformation, thereby reducing the solution to that of a 2×2 eigenvalue problem. The result corresponds to that of Zimmerman and Brittin,[58] which was obtained by Kärger for the analogous case of NMR field gradient experiments[56,57]

$$P(q_\Lambda,t) = P_s(q_\Lambda,t) + P_f(q_\Lambda,t) = p_s' \exp(-D_s' q_\Lambda^2 t) + p_f' \exp(-D_f q'^2_\Lambda t) \quad (16)$$

$$D_{s(f)}' = \frac{1}{2}\{D_s + D_f + q_\Lambda^{-2}(\tau_s^{-1} + \tau_f^{-1}) \mp \sqrt{[D_f - D_s + q_\Lambda^{-2}(\tau_f^{-1} - \tau_s^{-1})]^2 + 4q_\Lambda^{-4}\tau_s^{-1}\tau_f^{-1}}\} \quad (17)$$

$$p_f' = \{(p_s D_s + p_f D_f - D_s')\}/\{(D_f' - D_s')\}; \; p_s' = 1 - p_f' \quad (18)$$

In eq 17, the − and + signs correspond to D_s' and D_f', respectively.

4. Results

4.1. Phenomenological Line Shape Analysis. In the following, we will first look for signatures of the latex film formation in the line shapes of the FRS signals in a phenomenological, model-free manner. The tracer diffusion in homogeneous polymer melts a few degrees above the polymer glass transition temperature is known to proceed according to Fickian kinetics[59] in a homogeneous environment yielding exponential signal decays, eq 4, with inverse relaxation times τ^{-1}, which show the characteristic q^2 dependence, eq 6. In these cases the diffusion coefficients can be found from the slopes of τ^{-1} vs q^2 plots. In a drying latex dispersion the compartmentation of the material and the possibly inhomogeneous distribution of rest water in the polymer matrix can be expected to induce different degrees of hydroplasticization in different regions of the film and, concomitantly, to result in a spatial distribution of tracer diffusion coefficients. If these heterogeneities of environment subsist on length scales comparable to the grating distance Λ monitored by the FRS experiment, the signal decays will represent an average over this distribution leading to stretched exponential decay signals, as described by eq 5. In these cases, the relaxation time τ has to be replaced by the average $\langle\tau\rangle$ of the distribution (cf. Equation 6). In addition, the restrictions imposed on the diffusion paths of the (hydrophobic) tracer molecules by the microstructure of the drying film are anticipated to lead to deviations from Fickian diffusion, i.e., to deviation from the q^2 dependence of the average relaxation rate $\langle\tau\rangle^{-1}$, eq 6. Thus, the transition from a wet, heterogeneous polymer latex film to a dry homogeneous polymer film on drying should be visible in the FRS experiments by characteristic signatures: an increase of the line shape parameter from $\beta < 1$ to $\beta = 1$ and a change in the q dependence of the average relaxation rate, $\langle\tau\rangle^{-1} \propto q^x$, from non-Fickian diffusion ($x \neq 2$) to Fickian diffusion ($x = 2$).

To investigate the tracer diffusion in latex films in the course of drying, the decays of photoinduced gratings were measured in a broad range of grating distances Λ. The shapes of the decay kinetics as well as the dependence of the relaxation time on Λ were found to be substantially different at different stages of film formation. Figure 3 shows representative FRS signal decays of a drying latex film of P(BMA-*co*-1%AA) particles as function of the rest water content at constant grating distance $\Lambda = 0.8$ μm (Figure 3a) and as function of the grating distance at constant water content $C_{H_2O} = 7\%$ w/w (Figure 3b). On drying the decay kinetics slow and the line shapes change from significantly stretched to exponential. While the line shapes at low water content (2% and 3% w/w) can still be described by an exponential decay of the grating, eq 4 (dashed lines), the decay curves at high water contents (10 and 18% w/w) show a significant degree of stretching. A careful analysis of the line shapes in Figure 3a with a stretched exponential, eq 5, yields that while the average relaxation time $\langle\tau\rangle$ increases smoothly on drying (not shown) the stretching parameter increases continuously from values of $\beta \approx 0.8$ at the highest experimentally accessible water content (∼18% w/w) until it crosses over to a constant value $\beta = 1$ at a water content of ∼2% w/w as depicted in Figure 4a. With the uncertainties of the rest water contents in mind, one gets a first estimate for the water content at which a transition from a heterogeneous wet latex film to a homogeneous "dry"[69] polymer film takes place.

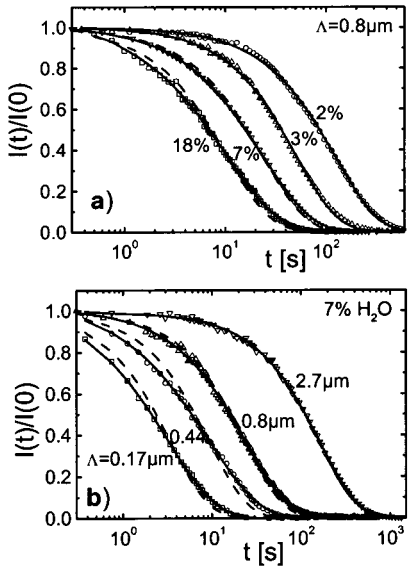

Figure 3. (a) Normalized FRS intensity decays, $I/I(0)$, employing gratings with $\Lambda = 0.8$ μm for ACR in the P(BMA-*co*-1%AA) latex film at different stages of drying. At higher water content (7−18% w/w) the kinetic curves deviate from exponential shape (dashed line, exponential fit, eq 4; solid line, stretched exponential fit, eq 5). In the case of low water content (2−3% w/w), the decay is exponential ($\beta = 1$). See Figure 4a for the resulting β-values. (b) Normalized FRS intensity decays, $I/I(0)$, for gratings with different spatial periods (Λ = 0.17, 0.44, 0.8, 2.7 μm) in the latex film of P(BMA-*co*-1%AA) particles (R = 101 nm) with 7% w/w of residual water. The solid lines are stretched exponential fits according to eq 5. $I(0)$ is just a fit-parameter (initial intensity). Exponential fits with eq 4 are shown in dashed lines.

Another characteristic signature of tracer diffusion in wet latex films is a pronounced length scale dependence of line shape and relaxation times. This is already visible in the raw data, Figure 3b, where the decay kinetics at a water content of 7% w/w are shown for several grating distances Λ. The line shapes evolve from rather exponential to significantly stretched curves when decreasing the length scale on which tracer motion is monitored from Λ= 2.7 μm to Λ = 0.173 μm. This length scale dependence increases on increasing the rest water content, while it disappears within experimental accuracy in dry films as demonstrated in Figure 4b where the Λ dependence of the line shape parameter β as obtained from fits with the stretched exponential function, eq 5, is depicted for several water contents. To reduce the significant scatter, averaging over several measurements and water contents was performed. A most intriguing feature is that the line shapes become exponential for grating distances $\Lambda > 2$ μm for all water

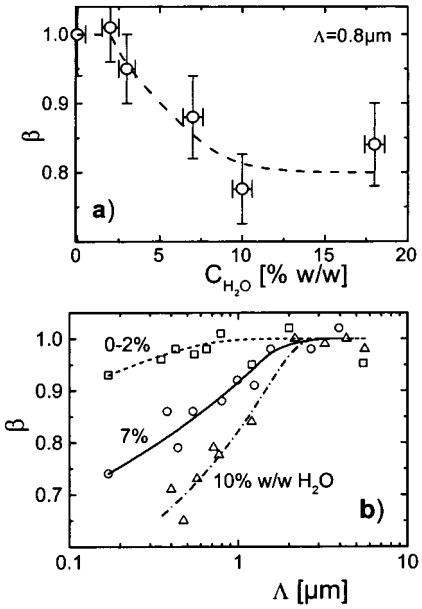

Figure 4. Stretching parameter β, describing the shape of FRS decay in terms of eq 5 (a) as a function of residual water concentration at a grating distance of $\Lambda = 0.8$ μm (cf. Figure 3a) and (b) drawn vs the grating distance, Λ, at different stages of film drying (residual water concentrations 10%, 7%, and 0−2% w/w).

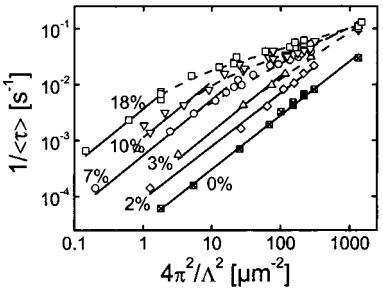

Figure 5. Mean grating decay rate $1/\langle\tau\rangle$ vs $q^2 = 4\pi^2/\Lambda^2$ (Λ: grating distance), at different stages of film formation (residual water concentrations C_{H_2O} are shown at the curves). Solid lines depict linear q^2 dependences (Fickian diffusion).

contents. In the qualitative picture used above this means that the heterogeneities in the latex films are most prominent on small length scales and disappear beyond a certain limiting length scale on which the latex film appears homogeneous again irrespective of the degree of drying.

In Figure 5 the q dependence of the relaxation times is compared to that of Fickian diffusion by plotting the inverse of the average relaxation time $\langle\tau\rangle^{-1}$ vs q^2 in a log−log representation. Fickian diffusion is symbolized by solid lines of unit slope. One clearly sees a transition from a Fickian tracer diffusion in dry or nearly dry polymer films to non-Fickian diffusion in wet latex films with the crossover water content being between 2 and 3% w/w in good agreement with the first estimate on the basis of the line shape parameters in Figure 4a. Intriguingly, a return to Fickian diffusion on large length scales (small q) is visible in the q dependence of the relaxation times as well. As in case of the Λ dependence of the β-parameter in Figure 4b this applies for grating distances Λ larger than 2 μm.

Another representation of the length scale dependence of tracer diffusion is the definition of an apparent diffusion coefficient, which has been determined accord-

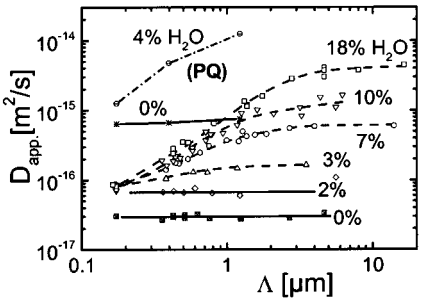

Figure 6. Apparent diffusion coefficient $D_{app} = \langle\tau\rangle^{-1}/(4\pi^2/\Lambda^2)$ of Aberchrome-540 in latex films of P(BMA-*co*-1%AA) particles ($R = 101$ nm) as a function of the grating distance, Λ, at different stages of film drying. The stages are indicated by water content (% w/w). Also shown is D_{app} of 9,10-phenanthrenequinone (PQ) in dry and wet films. Dashed lines represent fit results following the two-state model eq 20. Solid lines correspond to a constant D_{app} representing Fickian diffusion.

ing to eq 6, irrespective whether the diffusion process is of Fickian nature or not. As Figure 6 demonstrates this amounts to allowing for a length scale dependent apparent diffusion coefficient $D_{app}(\Lambda)$ for grating distances where diffusion becomes non-Fickian, while Fickian diffusion is signaled by D_{app} being constant. The advantage of this representation is that the concept of an apparent diffusion coefficient is more easily amenable to physical interpretation and comparison with possible diffusion models. When looking at Figure 6 and comparing dry and wet films, several striking features can be noticed. In dry or nearly dry films up to 2% w/w water content, the tracer diffusion can be described by a single, length-scale independent diffusion coefficient. Increasing the water content from 0 to 2% w/w leads to a uniform enhancement of the diffusion coefficient from $D = 3 \times 10^{-17}$ m^2/s (which is typical for dry polymer films of this type, irrespective of the production process[70]) to $D = 7 \times 10^{-17}$ m^2/s. At higher water content a length scale dependence sets in, which becomes the more pronounced the higher the water content. While the limiting value of D_{app} for the smallest detectable grating distances is rather unaffected by the water content and is essentially identical to the value obtained for the homogeneous film with 2% w/w water, the limiting value for large Λ increases by two and a half orders of magnitude. In addition, D_{app} tends to become Λ independent for large Λ. A qualitatively similar effect of long-scale diffusion enhancement was also found in experiments with another tracer—phenanthrenequinone (PQ)—in the same latex films, at a water content of 4% w/w (see Figure 6). Thus, the length scale-dependent enhancement of tracer diffusion seems to be a generic feature for hydrophobic tracer molecules.

The length scale dependence of the apparent diffusion coefficient can be used to study the effect of changing the formulation of the dispersion on the drying process. In Figure 7 the ratio of the limiting values of the apparent diffusion coefficient at high and low grating distances, $D_{sat} = D_{app}(\Lambda\rightarrow\infty)$ and $D_0 = D_{app}(\Lambda\rightarrow 0)$, respectively, is plotted as function of the rest water content for P(BMA) dispersions of varying acrylic acid content. On drying, this ratio decreases linearly (on a log−log scale) with decreasing water content, showing a sharp crossover to a value of one. At the corresponding water content a transition occurs from an inhomogeneous wet to a homogeneous "dry" latex film. This transition point is shifted to lower water contents, from

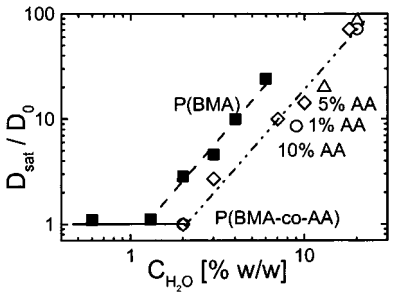

Figure 7. Water content dependence of the ratio of $D_{sat} = D_{app}(\Lambda\rightarrow\infty)$ to $D_0 = D_{app}(\Lambda\rightarrow 0)$ for a pure P(BMA) latex (■) and different acrylic acid contents (1, 5 and 10% w/w; ◇, △, and ○, respectively) in P(BMA-*co*-AA) latex films.

~2% to about 1%, when going from P(BMA-*co*-1%AA) to pure P(BMA) dispersions. This change can be well understood as the addition of acrylic acid into the polymer chains allows one to absorb more water homogeneously into the polymer bulk material than in case of the homopolymer. Surprisingly the addition of 5% and 10% acrylic acid into the formulation does not modify the drying behavior as compared to P(BMA-*co*-1%AA). The data points for the D_{sat}/D_0 ratio essentially superimpose. One possible explanation might be that the addition of more than 1% acrylic acid to the formulation does not lead to an increased incorporation of acrylic acid into the P(BMA) chains. The surplus acrylic acid is instead going most likely into the serum in form of acrylic acid homopolymer without significantly influencing the drying process. This result demonstrates that analysis of tracer diffusion in drying latex films may give access to details of material properties that are difficult to obtain otherwise. In addition, the clear-cut difference of the transition point in pure PBMA and P(BMA-*co*-AA) copolymers clearly indicates that the manner in which the water content was experimentally determined is less inaccurate than expected.

The most remarkable feature of tracer diffusion in wet latex films is its enhancement on large length scales. This is clearly incompatible with the existence of a barrier like in the model of barrier-impeded diffusion. The latter would lead to exactly the opposite length scale dependence of the tracer diffusion coefficient. Thus, the restriction that the tracer can diffuse only through the polymer phase has to be abandoned and the data are in the following analyzed within the more general two-state model.

4.2. Data Analysis with the Two-State Diffusion Model. To analyze the experimental results of Figure 6 with the two-state model, we need to obtain an expression for $D_{app}(\Lambda)$ within the model. For this purpose we evaluate

$$\tau_{app}^{(model)} = 1/(D_{app}^{(model)} q_\Lambda{}^2) = \int_0^\infty P(q_\Lambda,t)\,dt = p_s'/(D_s' q_\Lambda{}^2) + p_f'/(D_f' q_\Lambda{}^2) \quad (19)$$

and by use of eq 16 obtain $D_{app}^{(model)}$ as a function of $\Lambda = 2\pi/q_\Lambda$:

$$1/D_{app} = p_s'/D_s' + p_f'/D_f' \quad (20)$$

where $D_{s(f)}'$ and $p_{s(f)}'$ are given by eqs 17 and 18, respectively. To check if the model is able to reproduce the striking diffusional enhancement on large length scales, one can as a first step analyze the limiting behavior of $D_{app}(\Lambda)$. Noting that in order to significantly reduce the modulation amplitude of the optical grating the tracer needs to diffuse over a distance[71] of $\sqrt{\langle x^2\rangle} = \Lambda/2\pi$, one recognizes that the length scale $\Lambda_{crossover}$ of 1−2 μm, on which the crossover from short-distance, slow non-Fickian motion to large scale, fast Fickian diffusion takes place, corresponds to the order of the particle diameter (200 nm). We thus attribute the "slow" diffusion to transport of the tracer through the polymer core of the latex particles and assume that τ_s is approximated by the average time needed for a tracer to diffuse by a distance of the order of the latex sphere radius, R, i.e., $\tau_s = R^2/6D_s$. On diffusing over length scales $q_\Lambda{}^{-1} = \Lambda/2\pi \gg R$ (low q_Λ limit), the tracer molecule undergoes many exchange processes between latex particles and the interfacial membranes, which due to hydroplasticization allow for very fast motion with $D_f \gg D_s$. Therefore, the apparent diffusion coefficient in the limit $\Lambda \rightarrow \infty$ becomes the average

$$D_{sat} \equiv D_{app}(\Lambda\rightarrow\infty) = p_s D_s + p_f D_f \approx p_f D_f \quad (21)$$

In the opposite high q_Λ limit one finds

$$D_0 \equiv D_{app}(\Lambda\rightarrow 0) = D_s/p_s, \quad (22)$$

as follows from eqs 15, 16, and 20. Thus, if p_s and p_f are comparable, the two-state diffusion model reproduces the experimental behavior in the limits of motion over small and large distance (with respect to the particle size), i.e., $D_{sat} \gg D_0$.

To check if the two-state diffusion model is able to describe the complete length scale dependence of $D_{app}(\Lambda)$, the experimental data in Figure 6 were fitted with eq 20. As the four variable parameters necessary for the procedure of mean square deviation fit we chose the two root-mean-square displacements of the tracer in the two compartments $M_{s,f} = \sqrt{6D_{s,f}\tau_{s,f}}$ between the exchanges in addition to the two diffusion coefficients D_s and D_f. The advantage of this choice is that the root-mean-square displacements allow for a better visualization and interpretation of the transport processes in the film-forming latex dispersion (see below). The residence times $\tau_{s,f}$ and, through eq 12, the residence probabilities $p_{s,f}$ can then be calculated from the best fit values of the adjustable parameters.

The fit curves for $D_{app}(\Lambda)$ resulting from the two-state model are shown in Figure 6 (dashed lines). They reproduce the length scale dependence of the apparent diffusion coefficients quantitatively for all water contents. The best fit values of $D_{s,f}$ are plotted vs water content in Figure 8a, the corresponding $M_{s,f}$ are given in Figure 8b. Within some scatter diffusion in the slow environment does not change with water concentration as D_s and M_s turn out to be constant within experimental accuracy. In contrast the "fast" diffusion decelerates drastically in the course of film drying; whereas D_f noticeably exceeds D_s in wet latex films (by more than 2 orders of magnitude at a water content of 18% w/w), it collapses to the value of D_s in a narrow water content region around C_{H_2O} = 2% w/w. A similar behavior is exposed by the diffusional displacements of the tracer in the two compartments (Figure 8b). At the highest measurable water concentration, the "fast" displacement M_f is about four diameters of the latex particles. On drying, it shows a linear decrease by a factor of ~8 until it reaches the level of the displacement in the "slow" compartment at about 2% w/w water.

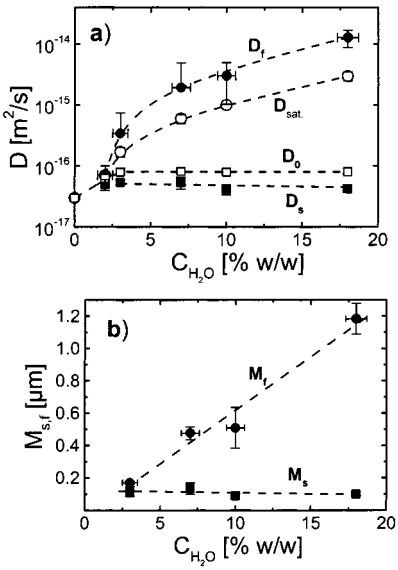

Figure 8. Water concentration dependence of the two-state model parameters for latex films of P(BMA-*co*-1%AA) particles (R = 101 nm): diffusion coefficients $D_{f,s}$ (a) and root-mean-square displacements $M_{f,s}$ (b) in "fast" (●) and "slow" (■) compartments. Also shown are experimentally acquired values of apparent diffusion in the limits of small (D_0, □) and large spatial periods of the grating (D_{sat}, ○).

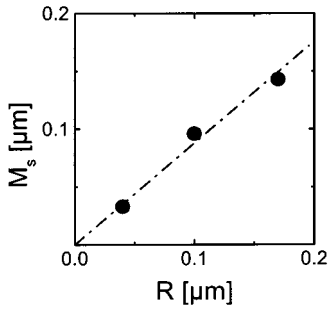

Figure 9. Correlation of the root-mean-square displacement in the slow domain, M_s, with the radius, R, of the latex particles. Three different dispersions of P(BMA-*co*-1%AA) (cf. Table 1) were examined. Linear regression leads to $M_s = (0.88 \pm 0.05)R$.

Also included in Figure 8a are the limiting values of the tracer diffusion coefficient for the smallest and the largest experimentally accessible grating distances, D_0 and D_{sat}, respectively, as read off from Figure 6. They can be considered to reasonably well approximate the theoretical limits $D_{app}(\Lambda \rightarrow 0)$ and $D_{app}(\Lambda \rightarrow \infty)$ as derived in eqs 21 and 22, respectively. Comparing the pairs D_s, D_0, and D_f, D_{sat} one finds that the predictions of eqs 21 and 22 are borne out by the experimental results: D_0 is higher as compared to D_s (cf. eq 22 with $p_s < 1$) and D_{sat} is smaller than D_f (cf. eq 21 with $p_f < 1$). Direct fits of the FRS decay curves according to eqs 15−18 yield essentially the same result for the model parameters shown in Figure 9.[60]

The values of $p_{s,f}$ can be obtained from the data and the fits by application of either eq 12 or eqs 21 and 22. As they are not independent parameters (cf. eq 12) only results for p_s are given in Table 2. One observes within considerable scatter a slight tendency to decrease from 1 to 0.7 with increasing water content.

A remarkable result of our data analysis is the absolute value of M_s: not only does it not change with water content, but its value of about 96 nm is close to the radius of the latex particles (R = 101 nm). To check if this is merely a fortuitous coincidence or if it has some deeper physical meaning, we varied the latex particle size and studied wet P(BMA-*co*-1%AA) latex films with particle radii R = 40 and 170 nm in addition. The corresponding $D_{app}(\Lambda)$ for a water content of 11 ± 1% w/w have been presented elsewhere[45] together with the fits according to eq 20. Here, we only restate that the data could again be quantitatively fitted. The variation of the resulting M_s with the particle radius R is depicted in Figure 9. The result is a clear linear correlation, $M_s \approx 0.88R$. This indicates that the near coincidence of M_s with the radius of the latex particles is systematic. Moreover, the finding that M_s is consistently found smaller than R by about 12% makes it very likely that the "slow phase" consists of the intact inner parts of the latex particles which show transport properties very similar to the correspondingly hydroplasticized bulk polymer (cf. the value of D_0 at zero water content in Figure 8a).

Table 2. Water Content Dependence of the Residence Probability p_s of the Tracer Dye for the Polymer Phase (Particles Cores) As Derived from Simultaneous Fits of the Length Scale Dependent Apparent Diffusion Coefficient $D_{app}(\Lambda)$ in Figure 6 (See Text)

water content (% w/w)	0	3	7	10	18
p_s	1	0.87 ± 0.08	0.74 ± 0.18	0.68 ± 0.16	0.67 ± 0.09

5. Discussion

Our results demonstrate that the analysis of the motion of a hydrophobic tracer provides intriguing insights into the changes of material properties of a drying latex film. From a model-free parametrization of the FRS decay signals one can deduce that on drying a transition occurs at a water content of 2 ± 0.5% w/w. Below this water content the films appear homogeneous on all length scales and the tracer transport proceeds via Fickian diffusion. The diffusion coefficients at about 2% w/w are increased by a factor of roughly two with respect to extensively dried films. The diffusion coefficients of these fully dried films were within experimental accuracy identical to those found for films obtained from the purified latex polymer either by solvent casting or by melt-pressing the polymer powder. The increase of the diffusion coefficient for not completely dried, but still homogeneous films is due to the effects of hydroplastization by water associated with the polar or charged groups on the polymer. The amount of 2% water that can be more or less homogeneously absorbed is in agreement with literature values for bulk polymers.[61,62]

When the water content was increased above 2% w/w, the latex films develop a characteristic length scale dependence of transport properties that is reflected in the line shape parameter β and the apparent diffusion coefficient D_{app} of tracer diffusion and accompanied by a deviation from the q^2 dependence of the relaxation rate τ^{-1} that defines Fickian diffusion. It is a remarkable signature of tracer diffusion in wet latex films that at large grating distances the film appears homogeneous again ($\beta = 1$; $\tau^{-1} \propto q^2$; $D_{app}(\Lambda) = \text{const.}$). The observation of exponential line shapes and Λ-independent diffusion coefficients at large Λ even in case of wet films precludes complementary gratings as the source of nonexponential decays and length scale dependent diffusion coefficients

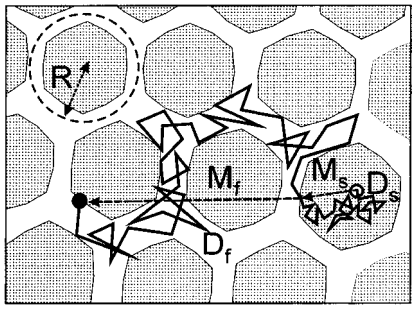

Figure 10. Visual representation of tracer diffusion in hydroplasticized (D_s) and hyperplasticized (D_f) compartments of a latex film according to experimental findings and the two-state model.

as these features should prevail at large Λ as well in this case.

The unusual behavior of tracer diffusion in wet latex films can instead be described as originating from the specific internal geometry of such films built from initially distinct latex particles and the effect of water. When the completely dried polymer latex films are rewetted with water, the characteristic length scale dependence of D_{app} reappears, even though the maximum achievable tracer diffusion enhancement at large grating distances Λ corresponds to only about 7% w/w water.[60] Contrastingly, plasticizing the sample with organic solvent does not result in a spatial period-dependent diffusion coefficient, even though the uniform enhancement of the tracer diffusion was much stronger than the effect of water at large Λ. Thus, the length scale dependent enhancement of tracer diffusion is a generic feature of latex films, connected to the presence of water.

This enhancement of tracer diffusion at large length scales was found to be irreconcilable with the concept of the hydrophilic membrane representing a barrier for the motion of the hydrophobic tracer used. Our observations were exactly opposite to the predictions of the barrier-impeded diffusion model which was successfully applied to analyze water diffusion in microemulsions.[55] However, a two-state diffusion model, assuming a distribution of the tracer between the polymer latex cores and the hydrophilic membrane, was able to successfully interpret the spatial scale-dependent diffusion observed in FRS experiments with latex films. The picture for tracer motion in the final stage of latex film drying that evolves from this model is summarized in Figure 10.

When the films are dried to a rest water content of 18% w/w, the colloidal particles have already come into contact and polymer fills almost the whole volume. In the course of further drying, the inner part of each colloidal particle keeps its size unchanged and stays moderately plasticized with water, the concentration of $\approx$2% w/w corresponding to the limits of solubility. These permanent cores (slow phase) are surrounded by a more hydrophilic layer of polymer enriched with hydrophilic groups, surface charges, surfactants, and salts. The excess of water above its normal solubility is thus contained in this layer, making it heavily plasticized, and the tracer diffusion in the "fast phase" drastically enhanced in comparison with its diffusion within the cores. Therefore the state of the interface compartment can be well characterized by the term "hyperplasticized". The spatial scale dependence of D_{app} reveals the contrast between the normal hydroplasticized and hyperplasticized areas of polymer; as the water content in the hyperplasticized phase decreases, the difference in water contents, and hence between D_s and D_f, lessens. Since the small-scale limiting diffusion coefficient D_0 is fully determined by (almost) constant D_s and p_s, it stays nearly constant, whereas the large-scale limit D_{sat} (related to D_f) rapidly decreases with water loss, until the values of D_0 and D_{sat} become equal. At this point (2% w/w water in P(BMA-*co*-1%AA) latex films) $D_f = D_s = D_0 = D_{sat}$, and further drying occurs uniformly in the whole bulk; at this stage the latex film cannot be distinguished from solvent-cast or melt-cast material by the FRS measurements.

To gain insight into the process of film formation on a microscopic level the model parameters p_f and p_s, which are derived from fits of tracer diffusion experiments, may seem to be the most relevant quantities. The increase of p_s from about 0.7 to 1 during drying as indicated in Table 2 could be taken as a measure of the changing relative size of the hyperplasticized interface and the particle cores. However, p_f and p_s, even though largely determined by geometrical volume fractions of fast and slow domains, have to be interpreted rather in terms of probabilities for the dye to be found in the respective phases. By eq 12, p_s and p_f are related to the residence times of the tracer in the respective phases. The residence times in a given phase will, however, also depend on the size of the contact area of the membranes between two neighboring latex particles, which will be changing on increasing the degree of particle deformation and thus be a function of the water content. In addition, differences in the affinity of the tracer dye with respect to the one or the other phase will affect the residence times. Thus one has to be careful not to overinterpret results obtained for $p_{s,f}$ by simply equating them to geometrical volume fractions. On the other hand, estimating the volume fraction of the slow phase (i.e., the particle cores) from the correlation coefficient 0.88 ± 0.05 between M_s and the particle radius via $p_s \propto M_s^3$ one obtains $p_s = 0.57-0.80$ in reasonable agreement with the saturation value of about 0.67 obtained by converting the fit results for M_s and D_s at water contents above 10% w/w into values for p_s. To address the question of the influence of specific tracer affinities tracer diffusion experiments where for given polymer latex film the polarity of the tracer dye is systematically varied would be required. Note that M_s has a simple geometrical interpretation and its value should thus be unaffected by affinities between tracer and compartment. The surprisingly good agreement (Figure 9) of M_s with the sphere radius, R, is the strongest support of the validity of the two-state model as a way to analyze tracer diffusion in wet latex films.

The used model, though it quite convincingly describes our experimental observations, has nevertheless to be considered as a rather crude and simplified zeroth order approximation of a complex process. In particular, the fact that the apparent diffusion coefficients have been derived from a line shape parametrization with a single stretched exponential, implying a continuous distribution of relaxation times, instead of a direct application of biexponential fits according to the two-state model may seem contradictory. However, it turned out that within experimental accuracy both approaches lead to the same results with respect to the water content dependence of the model parameters. On the other hand, there is no reason to assume that the

dynamics in either compartment needs to be described by a single diffusion coefficient. The origin for such a spatial heterogeneity in case of the polymer phase could be seen in an inhomogeneous distribution of charged and polar groups of the polymer. The concomitant inhomogeneous distribution of water would then lead to different regions of the particle cores being plasticized to different degrees resulting in a corresponding distribution of tracer mobilities. Such an inhomogeneous distribution of charged groups in a polymer is well described in the literature (ref 63 and references therein). On the other hand, it cannot be excluded that the polymer interdiffusion which is already taking place during drying at a temperature 5 K above the polymer T_g may lead to a spatially inhomogeneous modification of the transport properties of the interfacial membranes which in turn gives rise to a distribution of relaxation times. That such a modification is taking place can be inferred from the above-mentioned rewetting experiments, which show only a partial recovery of the length scale dependence of the apparent diffusion coefficient.

However, no preference could be given to any of the two scenarios on the basis of our data analysis, not to mention the possibility of a distribution of relaxation times in both phases. An incorporation of compartment inhomogeneity by generalizing the fit formula from biexponential to two stretched exponentials leads to the introduction of two additional parameters with concomitant overdetermination of fit parameters. For this reason we preferred to analyze, in terms of the two-state model, not the kinetic curves themselves but rather average characteristics extracted from them—namely, the conceptually easy to interpret grating distance-dependent apparent diffusion coefficient.

Notwithstanding these reservations, monitoring the diffusion of a (hydrophobic) tracer and analyzing either apparent diffusion coefficients or the corresponding Bragg signal relaxation functions within the simple two-state diffusion model appears to be an attractive approach to study the drying of polymer latex films. This approach allows one to probe the properties of both the latex particles cores and the internal particle/water interface, thus providing information on the drying process, especially the role of the particle interfaces, which is difficult to access otherwise. Thus it can complement other techniques that provide information about property changes of the film/air and film/substrate interfaces,[64] the interdiffusion of polymer chains and small molecules through the particle interfaces,[15,21] and the dynamics and distribution of water and surfactant molecules[63,65,66] in a nascent polymer latex film. As one example of the potential of this approach, we have shown in Figure 7 the effect on drying of changing the acrylic acid content of the latex. Complementing this with corresponding rewetting experiments[60] could help to establish a better understanding between the relationship of the formulation of a latex dispersion and the performance of the final latex film. This is of particular interest concerning the role of surfactants and other agents that modify the properties of the particle surfaces as the possibility of tailoring product properties by changing the particles surfaces is of increasing interest in industrial applications. In addition, modifying the hydrophobicity of the tracer dye will allow one to gain further knowledge on the effect and the fate of small molecules that are often present in latex films. The use of hydrophilic tracers may provide access to the properties of the aqueous compartments of a nascent latex film. Work along these lines is currently in progress.

6. Conclusion

We have demonstrated that monitoring the motion of a hydrophobic dye molecule by forced Rayleigh scattering in a drying polymer latex film allows one to obtain interesting insights into the drying process. The heterogeneity introduced by different compartments (polymer phase, aqueous phase, polymer/water interface) of a wet latex film and the partitioning of the dye between polymer phase and interface give rise to a tracer diffusion coefficient that appears to depend on the length scale monitored by the experiment. The enhancement of tracer diffusion on large length scales leads to the conclusion that the hydrophilic membranes surrounding the latex particles do not represent a barrier to the dye. By application of a two-state diffusion model, which takes into account a partitioning of the dye between a slow and a fast phase (attributed to the latex cores and the interfaces, respectively) the drying behavior could be quantitatively described. Even though this model has to be considered as a coarse grained description of a complex process, it allows one to trace the properties changes of two compartments of a drying latex film by assuming that a wet latex film consists of polymer cores, slightly plasticized by a small amount of absorbed water, and a connecting interfacial phase which is extensively plasticized (hyperplasticized) allowing for fast, long distance tracer motion. The drying is then described in terms of the water content dependence of model parameters such as diffusion coefficients (D_s, D_f), root-mean-square displacements (M_s, M_f), and residence probabilities (p_s, p_f) of the tracer in the two phases. For P(BMA-*co*-1%AA) dispersions, we found that on decreasing the water content from 18% to about 2% w/w the transport properties of the particle cores remain unchanged. Drying thus removes water from the interfacial areas first which results in an enormous decrease of the tracer diffusion coefficient D_f and the root-mean-square displacement M_f in the interfacial phase. At 2% water, where the length scale dependence of the apparent diffusion coefficient $D_{app}(\Lambda)$ was observed to disappear the transport properties of both compartments become equal and further drying results in a uniform reduction of the—now length scale independent—tracer diffusion coefficient to the value of the polymer melt. Significant support for the suggested model is derived from the clear-cut correlation between the root-mean-square tracer displacement in the slow phase M_s and the particle radius R; i.e., $M_s = 0.88\ R$.

In further work, we will use the approach presented to study the effect of modifying the properties of both the particles cores and the particle/water interface and apply it to the analysis of rewetting experiments with dried polymer latex films.

Acknowledgment. We thank A. Reichert and C. Lach (BASF AG) for preparation and characterization of the latex dispersions. Financial support by the Bundesministerium für Bildung und Forschung (BMBF) under contract No. 03D0060A5 is gratefully appreciated.

References and Notes

(1) Provder, T.; Winnik, M. A.; Urban, M. W., Eds. *Film formation in waterborne coatings*; ACS Symposium series 648; American Chemical Society: Washington, DC, 1996.

(2) Winnik, M. A. In *Emulsion polymerization and emulsion polymers*; Lovell, P. A., El-Aasser, M. S., Eds.; Wiley: New York, 1997; p 468.
(3) Winnik, M. A. *Curr. Opin. Colloid Interface Sci.* **1997**, *2*, 192.
(4) Visschers, M.; Laven, J.; German, A. L. *Prog. Org. Coat.* **1997**, *30*, 39.
(5) Keddie, J. L. *Mater. Sci. Eng. Rep.* **1997**, *21*, 101.
(6) Chevalier, Y.; Pichot, C.; Graillat, C.; Joanicot, M.; Wong, K.; Maquet, J.; Lindner, P.; Cabane, B. *Colloid Polym. Sci.* **1992**, *270*, 806.
(7) Hahn, K.; Ley, G.; Schuller, H.; Oberthür, R. *Colloid Polym. Sci.* **1986**, *264*, 1092.
(8) Crowley, T. L.; Sanderson, A. R.; Morrisoson, J. D.; Barry, M. D.; Morton-Jones, A. J.; Rennie, A. R. *Langmuir* **1992**, *8*, 2110.
(9) Rieger, J.; Hädicke, E.; Ley, G.; Lindner, P. *Phys. Rev. Lett.* **1992**, *68*, 2782.
(10) Rieger, J.; Dippel, O.; Hädicke, E.; Le, G. In *Colloidal polymer particles*; Goodwin, J. W., Buscall, R., Eds.; Academic Press: London, 1995; p 29.
(11) Joanicot, M.; Wong, K.; Cabane, B. *Macromolecules* **1996**, *29*, 4976.
(12) Chevalier, Y. *Trends Polym. Sci.* **1996**, *4*, 197.
(13) Wang, Y.; Juhué, D.; Winnik, M. A.; Leung, O. M.; Goh, M. C. *Langmuir* **1992**, *8*, 760.
(14) Kim, H.-B.; Winnik, M. A. *Macromolecules* **1995**, *28*, 2033.
(15) Feng, J.; Winnik, M. A. *Macromolecules* **1997**, *30*, 4324.
(16) Juhué, D.; Lang, J. *Langmuir* **1993**, *9*, 792.
(17) Butt, H.-J.; Kuropka, R.; Christensen, B. *Colloid Polym. Sci.* **1994**, *272*, 2, 1218.
(18) Lin, F.; Meier, D. J. *Langmuir* **1995**, *11*, 2726.
(19) Juhue, D.; Wang, Y. C.; Lang, J.; Leung, O. M.; Goh, M. C.; Winnik, M. A. *J. Polym. Sci. B* **1995**, *33*, 1123.
(20) Lin, F.; Meier, D. J. *Langmuir* **1996**, *12*, 2774.
(21) Baumgart, T.; Cramer, S.; Jahr, T.; Veniaminov, A.; Adams, J.; Fuhrmann, J.; Jeschke, G.; Wiesner, U.; Spiess, H. W.; Bartsch, E.; Sillescu, H. *Macromol. Symp.* **2000**, *151*, 451.
(22) Eichler, H. J.; Günther, P.; Pohl, D. W. *Laser-Induced Dynamic Gratings* Springer: Berlin, 1986.
(23) Sillescu, H.; Ehlich, D. In *Lasers in Polymer Science and Technology*; Fouassier, P., Rabek, J. F., Eds.; CRC Press: Boca Raton, FL, 1990; p 211.
(24) Antonietti, M.; Coutandin, J.; Grütter, R.; Sillescu, H. *Macromolecules* **1984**, *17*, 798.
(25) Bartsch, E.; Frenz, V.; Möller, S.; Sillescu, H. *Physica A* **1993**, *201*, 363.
(26) Wang, C. H.; Xia, J. L. *J. Chem. Phys.* **1990**, *92*, 2603.
(27) Wang, C. H.; Xia, J. L.; Yu, B. K. *Macromolecules* **1991**, *24*, 3638.
(28) Zhang, J.; Yu, B. K.; Wang, C. H. *J. Phys. Chem.* **1986**, *90*, 1299.
(29) Veniaminov, A. V.; Sedunov, Y. N. *J. Polym. Sci., Ser. A* **1996**, *38*, 59.
(30) Heuberger, G.; Sillescu, H. *J. Phys. Chem.* **1996**, *100*, 15255.
(31) Lashkov, G. I.; Veniaminov, A. V.; Ratner, O. B. *Polym. Sci. USSR* **1986**, *28*, 487.
(32) Veniaminov, A. V.; Burunkova, Y. E.; Kazannikova, A. V. *Int. Polym. Sci. Technol.* **1989**, *16*, 109.
(33) Veniaminov, A. V.; Sillescu, H. *Macromolecules* **1999**, *32*, 1828.
(34) Zielinski, J. M.; Heuberger, H.; Sillescu, H.; Wiesner, U.; Heuer, A.; Zhang, Y.; Spiess, H. W. *Macromolecules* **1995**, *28*, 8287.
(35) Ehlich, D.; Takenaka, M.; Okamoto, S.; T. Hashimoto, T. *Macromolecules* **1993**, *26*, 189.
(36) Ehlich, D.; Takenaka, M.; Hashimoto, T. *Macromolecules* **1993**, *26*, 492.
(37) Dalvi, M. C.; Lodge, T. P. *Macromolecules* **1993**, *26*, 859.
(38) Eastman, C. E.; Lodge, T. P. *Macromolecules* **1994**, *27*, 5591.
(39) Dalvi, M. C.; Lodge, T. P. *Macromolecules* **1994**, *27*, 3487.
(40) Rappon, M.; Ghazalli, K. M. *Eur. Polym. J.* **1995**, *31*, 233.
(41) Rappon, M.; Ghazalli, K. M. *Eur. Polym. J.* **1995**, *31*, 1185.
(42) Rappon, M.; Ghazalli, K. M.; Rochanakij, S. *Eur. Polym. J.* **1997**, *33*, 1689.
(43) Kardinahl, T.; Franke, H. *Appl. Phys. A, Mater. Sci. Proc.* **1995**, *61*, 23.
(44) Veniaminov, A. V.; Sillescu, H. *Chem. Phys. Lett.* **1999**, *303*, 499.
(45) Bartsch, E.; Jahr, T.; Veniaminov, A.; Sillescu, H. *J. Phys. IV Fr.* **2000**, *10*, 289.
(46) DosRamos, J. G.; Silebi, C. A. *J. Colloid Interface Sci.* **1990**, *135*, 165.
(47) Johnson, C. S. *J. Opt. Soc. Am. B* **1985**, *2*, 317.
(48) Rhee, K. W.; Gabriel, D. A.; Johnson, C. S. *J. Phys. Chem.* **1984**, *88*, 8, 4010.
(49) Park, S.; Sung, J.; Kim, H. *J. Phys. Chem.* **1991**, *95*, 5, 7121.
(50) Kogelnik, H. *Bell Syst. Technol. J.* **1969**, *48*, 2909.
(51) Collier, R. J.; Burckhardt, C. B.; Lin, L. H. *Optical Holography*; Academic Press: New York, 1971.
(52) Hamad, A. Y.; Wicksted, J. P. *Opt. Commun.* **1997**, *138*, 254.
(53) Moharam, M. G.; Gaylord, T. K.; Magnusson, R. *J. Opt. Soc. Am.* **1980**, *70*, 300.
(54) Martin, S. C.; Singh, N.; Wallace, S. C. *J. Phys. Chem.* **1996**, *100*, 8066.
(55) Balinov, B.; Linse, P.; Soderman, O. *J. Colloid Interface Sci.* **1996**, *182*, 539.
(56) Kärger, J. *Ann. Physik (Leipzig)* **1969**, *24*, 1.
(57) Kärger, J.; Pfeifer, H.; Heink, W. *Adv. Magn. Reson.* **1988**, *12*, 1.
(58) Zimmerman, J. R.; Brittin, W. E. *J. Chem. Phys.* **1957**, *61*, 1328.
(59) Ehlich, D.; Sillescu, H. *Macromolecules* **1990**, *23*, 1600.
(60) Veniaminov, A.; Jahr, T.; Sillescu, H.; Bartsch, E. To be published.
(61) Iordanskii, A. L.; Rudakova, T. E.; Zaikov, G. E. *Interaction of Polymers with Bioactive and Corrosive Media*; VSP: Utrecht, The Netherlands 1994.
(62) Saechtling, H.; Oberbach, K.; Pabst, F. *Kunststoff Taschenbuch*; Hanser Fachbuch: Munich, Germany, 1998.
(63) Rottstegge, J.; Landfester, K.; Wilhelm, M.; Spiess, H. W.; Heldmann, C. *Colloid Polym. Sci.* **2000**, *278*, 236.
(64) Holl, Y. *Macromol. Symp.* **2000**, *151*, 473.
(65) Wallin, M.; Glover, P. M.; Hellgren, A. C.; Keddie, J. L.; McDonald, P. J. *Macromolecules* **2000**, *33*, 8443.
(66) Ciampi, E.; Goerke, U.; Keddie, J. L.; McDonald, P. J. *Langmuir* **2000**, *16*, 1057.
(67) Note that the molar ratio of BMA and AA was erroneously quoted as 99:1 in ref 45.
(68) The FRS data were quantitatively analyzed in terms of the barrier-impeded model described by Balinov et al.[55] Strong deviations from the predicted behavior of the apparent diffusion coefficient were observed, so that we discarded this model in our study.
(69) As the transition marked by a significant change in tracer motion occurs at a rest water content of 2% w/w, "dry" means nearly dry and takes into account further (homogeneous, see below) drying to the final latex film.
(70) The same diffusion coefficients were found within experimental accuracy in completely dry materials for films produced in different ways: by casting the purified latex polymer from toluene solutions, by melt-pressing the purified latex polymer, or by drying the corresponding latex dispersion.
(71) Spatial scale of FRS experiment: $\sqrt{\langle x^2\rangle} = \Lambda/2\pi$ is a realistic measure of the root-mean-square displacement, $\sqrt{\langle x^2\rangle} = \sqrt{2Dt}$, as it corresponds to a decrease of the grating efficiency to e^{-1}: $\exp(-8\pi^2 Dt/\Lambda^2) = \exp(-4\pi^2\langle x^2\rangle/\Lambda^2) = e^{-1}$ (cf. eq 4).

MA010531N